THE JOURNAL OF PHYSICAL CHEMISTRY LETTERS
A JOURNAL OF THE AMERICAN CHEMICAL SOCIETY

pubs.acs.org/JPCL

Letter

Polariton Decay in Donor–Acceptor Cavity Systems

Courtney A. DelPo, Saeed-Uz-Zaman Khan, Kyu Hyung Park, Bryan Kudisch, Barry P. Rand, and Gregory D. Scholes*

Cite This: *J. Phys. Chem. Lett.* 2021, 12, 9774–9782

Read Online

ACCESS | Metrics & More | Article Recommendations | Supporting Information

ABSTRACT: Enhanced delocalization is beneficial for absorbing molecules in organic solar cells, and in particular bilayer devices, where excitons face small diffusion lengths as a barrier to reaching the charge-generating donor–acceptor interface. As hybrid light–matter states, polaritons offer exceptional delocalization which could be used to improve the efficiency of bilayer organic photovoltaics. Polariton delocalization can aid in delivering excitons to the donor–acceptor interface, but the subsequent charge transfer event must compete with the fast decay of the polariton. To evaluate the viability of polaritons as tools to improve bilayer organic solar cells, we studied the decay of the lower polariton in three cavity systems: a donor only, a donor–acceptor bilayer, and a donor–acceptor blend. Using several spectroscopic techniques, we identified an additional decay pathway through charge transfer for the polariton in the bilayer cavity, demonstrating charge transfer from the polariton is fast enough to outcompete the decay to the ground state.

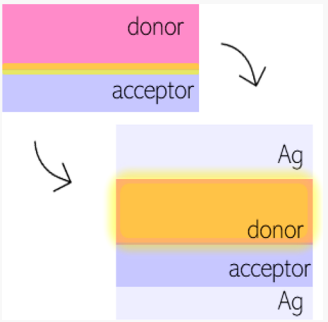

Strong light–matter coupling in cavities produces new collective excitation states known as polaritons. Owing to their extraordinary delocalization in the molecule basis and modified energy levels, polaritons offer an interesting avenue for the optimization of material properties with demonstrated success in long-range energy transfer,[1−4] increased conductivity and photoconductivity of organic semiconductors,[5,6] and enhanced rate and barrier free reverse intersystem crossing.[7,8] The structure of the light–matter Hamiltonian matrix produces a partly photonic character of a polariton state and leads to a marked improvement in delocalization compared to a purely molecular exciton state.[9−11] The delocalization of the polariton has been theoretically predicted and experimentally demonstrated to improve exciton and charge transport which are essential properties in organic solar cells (OSC).[12−18] Various other forms of light–matter coupling including surface plasmons and plasmonic nanoparticles and nanowires have been incorporated into photovoltaics to successfully improve device performance.[19−25]

In an OSC, the donor (or acceptor) molecule must transport excitons to the donor–acceptor interface to generate charges.[26] The exciton diffusion length, L_D, of an organic semiconductor is typically 5−10 nm, necessitating the use of a bulk heterojunction architecture where the donor and acceptor molecules are present in intermixed domains.[27,28] However, the bilayer architecture has the advantage of allowing for separate optimization of the morphology of the donor and acceptor layers as well as more efficient charge collection.[29−32] If exciton transport could be improved to reach lengths commensurate with the absorber layer thickness (for maximal absorption of sunlight ∼50−100 nm), the bilayer architecture could become competitive with the bulk heterojunction architecture.

Theoretical studies have indicated that exciton transport inside an electronically coupled system might occur across the entire length of the cavity because the delocalized polariton can be robust to shallow defects or disorder in the system.[14,15] An implication of such models is that excitons in a donor–acceptor bilayer cavity system are anticipated to be transported to the donor–acceptor interface with higher efficiency than in an uncoupled bilayer system. However, it is not guaranteed that more excitons at the interface will lead to the generation of more charges and higher cell efficiency.

In an uncoupled bilayer system, the decay of the exciton to the ground state competes with the rate of exciton transport to the interface. This competition is quantified through the exciton diffusion length, $L_D = (D\tau)^{1/2}$, where D is the diffusion coefficient and τ is the exciton lifetime.[33] Excitons formed within distances of the donor–acceptor interface that are greater than L_D will decay to the ground state. In a bilayer with a donor material thickness of ∼100 nm and a corresponding L_D of 5−10 nm, the majority of the excitons formed decay to the ground state. For the fraction of excitons that do reach the interface, charge transfer is a very fast and favorable process. In contrast, in a bilayer cavity system, the exciton transport is predicted to be extremely efficient such that all excitons should

Received: August 11, 2021
Accepted: September 29, 2021
Published: October 1, 2021

https://doi.org/10.1021/acs.jpclett.1c02644
J. Phys. Chem. Lett. 2021, 12, 9774–9782

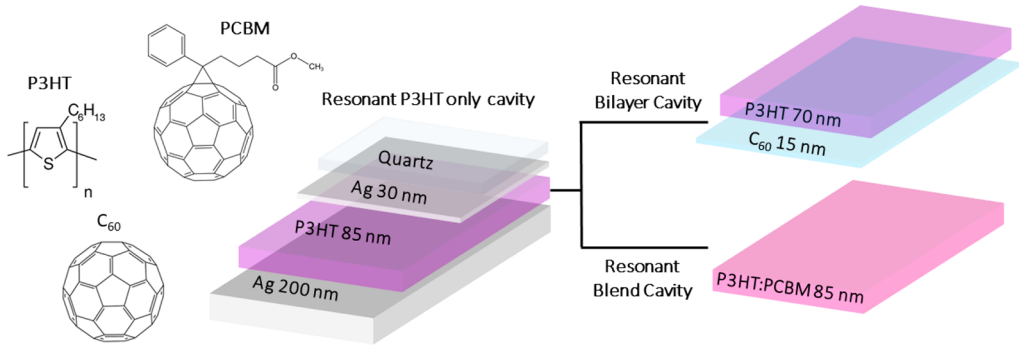

Figure 1. Structures of the donor molecule (P3HT) and acceptor molecules (C_{60}, PCBM) and the architectures of the P3HT cavity, the P3HT/C_{60} bilayer cavity, and the P3HT:PCBM (1:0.25) blend cavity. The P3HT:PCBM ratio was selected to be close to the P3HT/C_{60} ratio in the bilayer. All cavities are coupled to an electronic transition of the P3HT donor molecule. C_{60} is compatible with thermal evaporation for a bilayer while PCBM has additional functional groups making it compatible with spin-coating in a blend. The bilayer is intentionally nonoptimal for charge transfer outside of the cavity with a P3HT layer thickness that is much greater than the exciton diffusion length of P3HT.

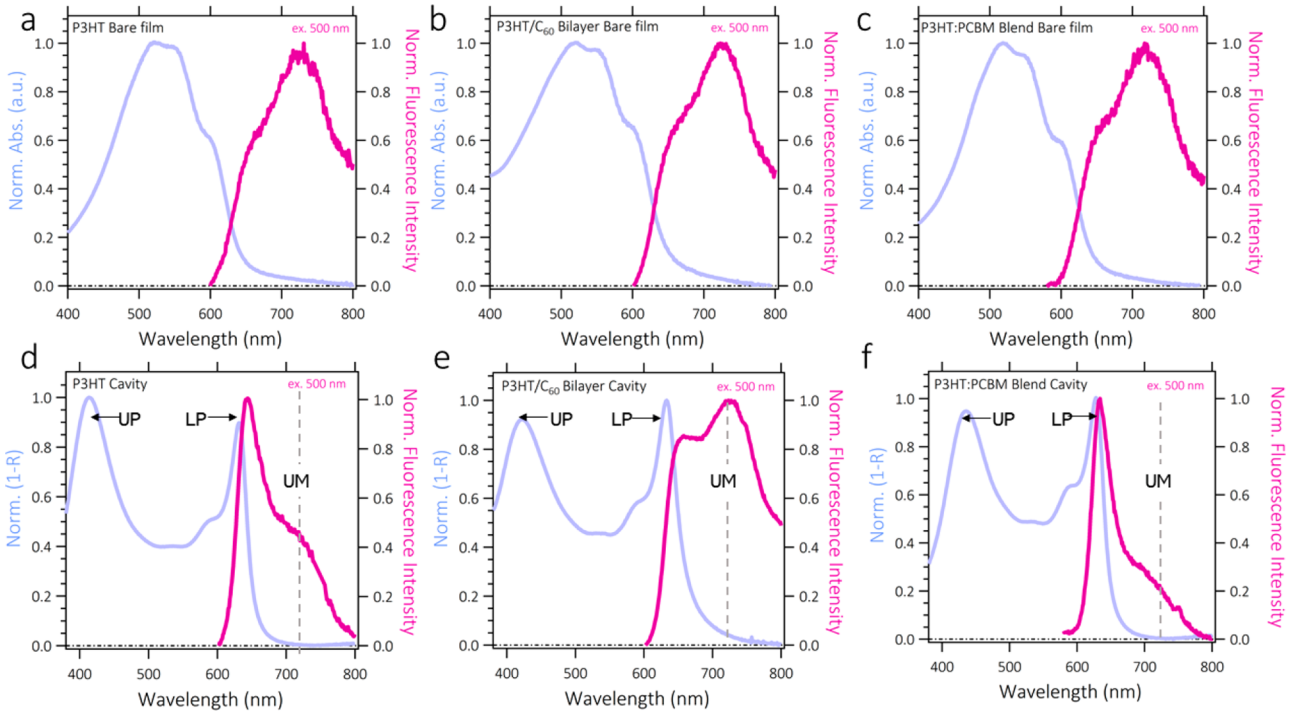

Figure 2. Steady-state characterization of the cavity systems and bare film controls. Absorption and fluorescence of the bare P3HT film (a), the bare P3HT/C_{60} bilayer film (b), the bare P3HT:PCBM blend film (c), and the corresponding cavity systems (d–f). All cavity systems are reflective such that $A = 1 - R$ (Figure S5). The fluorescence of the P3HT/C_{60} bilayer cavity (e) displays prominent contribution from uncoupled molecules (UM), which is in contrast to the LP dominated fluorescence of the P3HT cavity (d) and the P3HT:PCBM blend cavity (f). Gray dashed lines in (d–f) are placed at the fluorescence peak of UM, and UP and LP energies are designated with arrows. All cavity measurements are obtained at ~10°.

reach the interface irrespective of the distance from the donor–acceptor interface. However, at the interface, there is a competition between charge transfer from the polariton and the decay of the polariton to the ground state. The strong delocalization of the polariton has been implicated in slowing the rate of a transition between a hybrid light–matter polariton and a purely matter state,[34−36] and so we anticipate a slower rate of charge transfer to the acceptor from the polariton. Concurrently, we anticipate a very fast decay of the polariton to the ground state. If the rate of charge transfer is slower than the decay of the polariton to the ground state, charge transfer will not occur and no charges will be generated. While the polariton can improve the number of excitons that reach the donor–acceptor interface, it must first be demonstrated that charge transfer is a viable decay pathway for the polariton before polaritons can be used to improve the overall efficiency of bilayer organic photovoltaics.

In this study, we compare three cavity systems relevant to organic solar cell active layers, in all cases where the cavity resonance is tuned to an electronic transition of the donor: a donor only, a donor–acceptor bilayer, and a blend (Figure 1). The donor system is P3HT (regioregular poly(3-hexylthiophene-2,5-diyl)), and we incorporated a C_{60}-type fullerene acceptor (C_{60} or PCBM [6,6]-phenyl-C_{61}-butyric acid methyl ester). Through comparison of the spectroscopic properties of these cavity systems, we demonstrate charge transfer from the

https://doi.org/10.1021/acs.jpclett.1c02644
J. Phys. Chem. Lett. 2021, 12, 9774−9782

lower polariton can compete with the decay of the polariton to the ground state. However, for the donor−acceptor combination presented here, the charge generation efficiency of the lower polariton in the bilayer cannot compete with the efficiency of the charge generation from uncoupled molecules in the blend (bulk heterojunction). While further optimization of the polariton properties is required, this study establishes the potential for polaritons to improve the efficiency of organic photovoltaics.

We start by documenting the results of steady-state spectroscopic studies of the P3HT, P3HT/C_{60} bilayer, and bare (in the absence of a cavity) P3HT:PCBM blend films (Figure 2a−c) and cavity systems (Figure 2d−f). The P3HT film has a maximum absorption at 515 nm with vibronic shoulders at 560 and 605 nm and a maximum fluorescence peak at 730 nm with a shoulder at 660 nm (Figure 2a), an indication of crystalline H-aggregate formation.[37−39] The absorption and fluorescence of the P3HT/C_{60} bilayer and P3HT:PCBM blend bare films are approximately the same as those of the bare film of P3HT in the visible region. Both PCBM and C_{60} predominantly absorb in the UV region and do not couple to the cavity mode.[40,41] We note that, in contrast to the bare blend film, the structure for the bare bilayer film is intentionally nonoptimal for charge generation with a donor layer thickness (∼70 nm) that is significantly larger than the exciton diffusion length of P3HT (∼8 nm).[42]

Following incorporation into the Fabry−Perot architecture, the steady-state spectra of these molecular layers change drastically (Figure 2d−f). Here, we targeted the 0−2 vibronic transition (515 nm) of P3HT for coupling the Fabry−Perot cavity resonance in all three systems; however, the exact cavity energy varied for the three systems between 500 and 515 nm. To verify the avoided crossing formed by strong coupling between the electronic transition and an optical cavity mode, we plot the reflection spectra for a series of cavities of varying thicknesses (Figure 3). By analyzing the peak positions using the coupled oscillator model (see the inset of Figure 3 and the Supporting Information for details), we were able to confirm that the high- and low-energy peaks correspond to the upper (UP) and lower (LP) polariton peaks, respectively, and the cavity resonance coincides with the P3HT electronic transition at an optimized thickness of 85 nm with a refractive index of $n_{eff} \sim 3$.

The values for the Rabi splitting and exciton and cavity energies for each of the cavity systems were also extracted from fits of the angle-dependent reflectivity in the same manner (Figures S1−S3). The P3HT cavity system has an upper polariton (UP) absorption at 415 nm and a lower polariton (LP) absorption at 630 nm. The Rabi splitting for this system was calculated to be ∼1.03 eV, which corresponds to ∼40% of the energy of the P3HT electronic transition, placing this cavity system in the ultrastrong coupling regime. The Rabi splitting for the P3HT/C_{60} bilayer cavity is approximately the same as that for the P3HT only cavity system at ∼0.99 eV with an UP absorption at 425 nm and an LP absorption at 635 nm. The Rabi splitting for the P3HT:PCBM cavity system is slightly smaller at ∼0.88 eV with a UP at 435 nm and an LP at 625 nm but nevertheless remains in the ultrastrong coupling regime. The angle-dependent reflection has been known to exhibit a relatively flat dispersion that is not immediately recognized as an avoided crossing.[5] We attribute this to the high refractive index of the cavity, which, within the range of incident angles tested, gives a smaller variation of the cavity

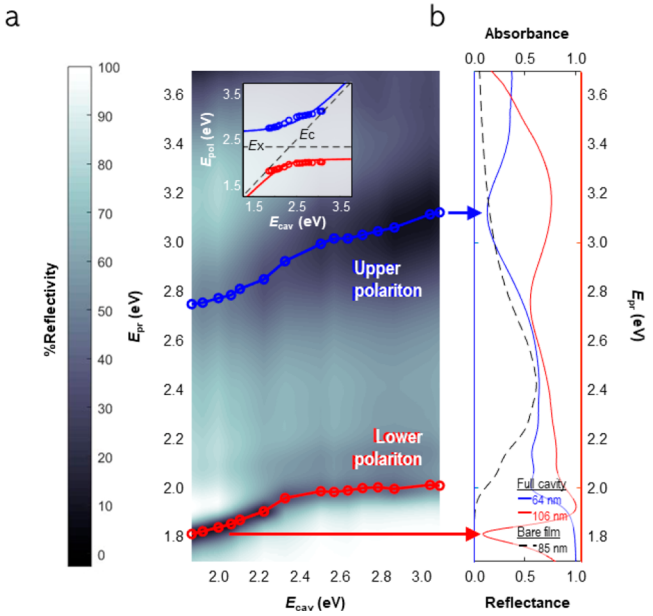

Figure 3. (a) Thickness-dependent reflectivity of P3HT/C_{60} bilayer cavities. The cavity mode energy, E_{cav}, increases with increasing thickness of the cavity, and the avoided crossing is realized near the resonant condition where the exciton energy, E_x, is equal to E_{cav}. The inset shows the extrapolated fit of the data using the coupled oscillator model. (b) Reflectance of the thinnest (blue-shifted resonance, blue curve) and thickest (red-shifted resonance, red curve) cavities with the absorption of the bare film for reference (black dashed curve).

mode energy compared to that of the wider thickness range examined to verify the avoided crossing (Figure 3).

The fluorescence spectra for the P3HT and P3HT:PCBM blend cavity systems feature a sharp fluorescence peak adjacent to the LP peak from the reflectivity spectrum along with broader shoulder peaks at longer wavelengths. We assign the sharp fluorescence peak as LP fluorescence and the remaining feature as an underlying smaller contribution from uncoupled molecules (Figure 2d,f). The contribution from uncoupled molecules is smallest in the blend cavity where the fluorescence of uncoupled molecules is most efficiently quenched. In contrast, the fluorescence of the bilayer cavity features a more prominent contribution from uncoupled molecules (Figure 2e) with a fluorescence spectrum that more closely resembles the bare bilayer film fluorescence (Figure 2b). The dominance of the uncoupled molecules in the bilayer cavity fluorescence occurs only for resonantly coupled systems (Figure S4).

To understand the excited-state dynamics that contribute to the differences observed in the LP fluorescence and, furthermore, in the charge generation process, we performed transient reflection spectroscopy on the cavity systems. We varied excitation wavelengths to find that the cavity dynamics are significantly modified by strong coupling. Before delving into the kinetic analysis to demonstrate how the excited-state dynamics can vary by tuning the excitation energy, we first clarify the accessible states at each of the excitation wavelengths.

In the strongly coupled system, coupling the absorption of N number of molecules to one cavity mode leads to the formation of $N + 1$ number of states: two bright states at new energy levels, the UP and LP, as well as a manifold of $N - 1$ dark states (DS) that remain at the energy level of the coupled absorption.[43] While the transition from the ground

https://doi.org/10.1021/acs.jpclett.1c02644
J. Phys. Chem. Lett. 2021, 12, 9774−9782

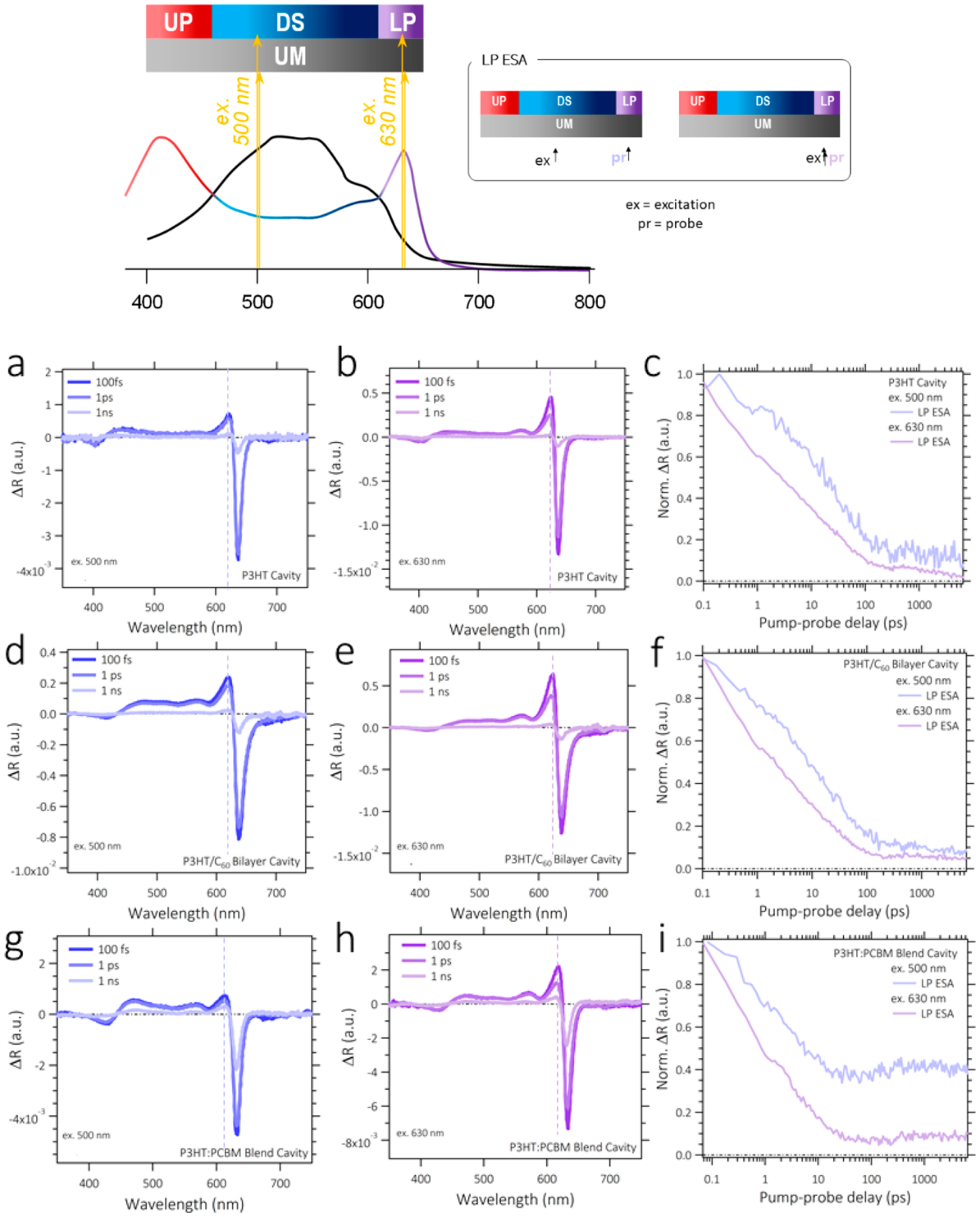

Figure 4. Resonant condition is confirmed through the excitation wavelength-dependent dynamics of the LP ESA. Top graphic demonstrates the absorbers at each of the excitation wavelengths with overlaid absorption spectra for a cavity and bare film and outlines the LP ESA. Transient reflection spectra and selected dynamics for the P3HT cavity (a–c), the P3HT/C_{60} bilayer cavity (d–f), and the P3HT:PCBM blend cavity (g–i). The LP ESA is designated with a blue (ex. 500 nm, a, d, g) or purple (ex. 630 nm, b, e, h) vertical dashed line with the corresponding dynamics in blue and purple traces (c, f, i). Excitation at the LP energy leads to a faster decay of the LP ESA (purple trace in c, f, i) as compared to the decay of the LP ESA with excitation at 500 nm (blue trace in c, f, i) in each of the resonant cavities. The power density for all transient measurements was 7.9 μJ cm^{-2}.

state to the dark states is largely optically dark, the dark states can be populated through the polariton states as well as other excited states of the system so we anticipate signatures of the dark states in the transient reflection data. We excite the cavity systems at the energy of the dark states and uncoupled absorbers (500 nm) and at the LP energy (630 nm). As shown in Figure 4, the broad absorption of P3HT overlaps with the cavity absorption, so at either excitation wavelength we excite

https://doi.org/10.1021/acs.jpclett.1c02644
J. Phys. Chem. Lett. 2021, 12, 9774–9782

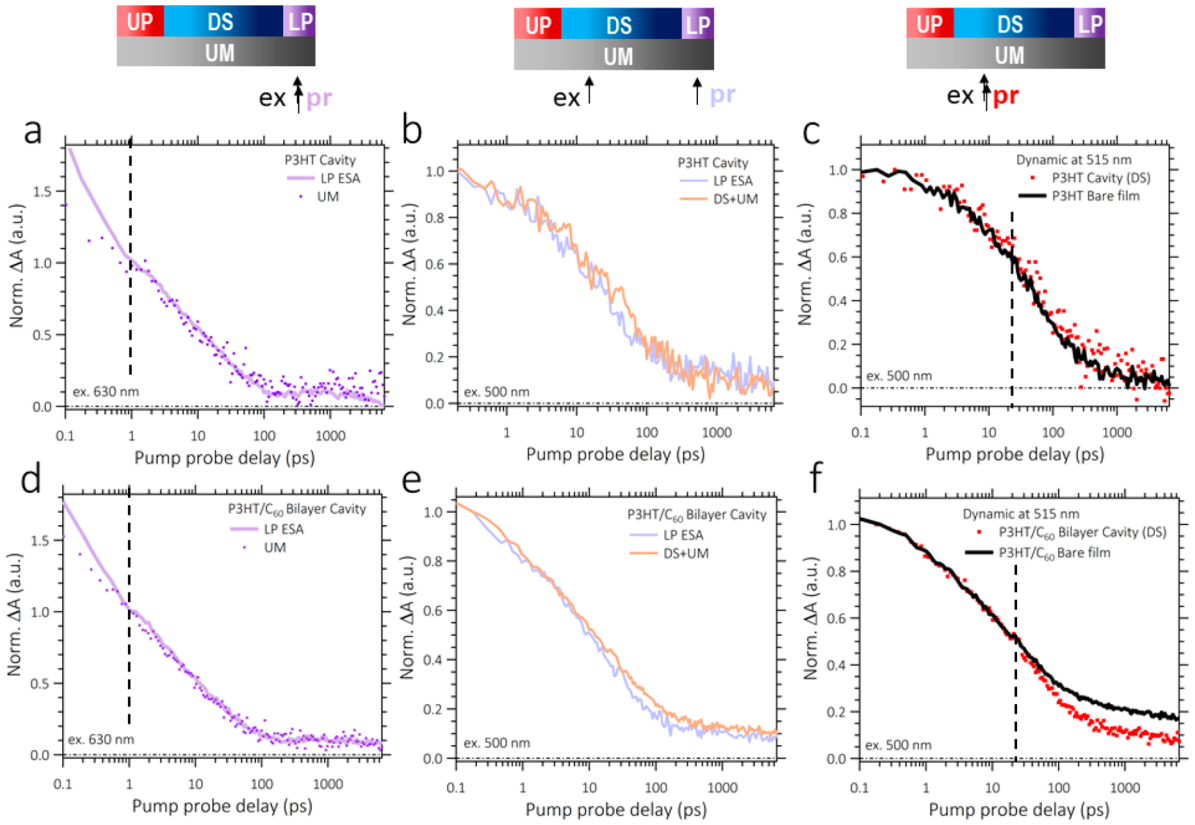

Figure 5. LP ESA contains contributions from the LP and UM (DS and UM) when excited at 630 nm (500 nm). (a, d) LP ESA dynamics (solid) and UM dynamics (dotted) with 630 nm excitation normalized at 1 ps (black dashed line placed at 1 ps). (b, e) LP ESA dynamics (blue) and DS + UM dynamics (orange) with 500 nm excitation normalized at 100 fs. (c, f) Dynamics at 515 nm for the DS inside the cavity (red dotted) and the UM bare film (black) normalized at 100 fs (black dashed line placed at 25 ps). Bare film and cavity transient measurements were recorded under the same power density, 7.9 μJ cm^{-2}.

both the cavity states and the uncoupled molecules (UM). The UM are the primary absorbers at 500 nm, while the LP and UM are the primary absorbers at 630 nm. In accordance with recent reports,[43−45] our pump−probe experiments differentiate between the dark state (DS) and UM populations. The UM dynamics here specifically refer to the dynamics of the bare film at a given wavelength. The bare film dynamics of P3HT depend on the probe−pulse wavelength because of the interplay of several excited-state species (excitons, polarons, etc.), whereas the DS dynamics are kinetically coupled specifically to the exciton dynamics as well as to the LP state.

The transient reflection data feature a broad derivative-like feature at the energy of the UP and a sharp derivative-like feature at the energy of the LP with positive signal from the DS in between the two features. Here we focus on the excitation wavelength-dependent dynamics of the excited-state absorption (ESA) probed at the energy of the LP which we refer to hereafter as the "LP ESA". We observe a faster decay of the LP ESA when exciting the systems at the energy of the LP (purple trace in Figure 4c,f,i compared to the decay of the LP ESA when exciting at the reservoir energy (blue trace in Figure 4c,f,i). This occurs only for the resonant cavity systems (Figure S10). On the basis of previously established assignments of the spectral features of ultrastrong cavity systems in transient reflection spectroscopy, we can anticipate contributions from the LP, DS, and UM populations to the kinetic evolution of this LP ESA feature.[46]

When exciting the cavity systems at the LP energy, we observe the dynamics of the primary absorbers at this wavelength, the LP and UM. We resolve a fast decay of the LP state within 1 ps followed by the dynamics of the UM. At 1 ps, we normalize the dynamics of the LP ESA (solid line, Figure 5a,d) with the dynamics of the UM at the same wavelength (dotted line, Figure 5a,d) to highlight the faster decay before 1 ps and the overlap after 1 ps. Similarly, when exciting the cavity systems at 500 nm, we observe contributions from the two primary absorbers at this wavelength, the DS and UM. The LP ESA trace (blue, Figure 5b,e) is best approximated by overlapping contributions from the independent DS and UM decay profiles at the LP ESA wavelength scaled to their relative intensities outside of the cavity system (orange trace, Figure 5b,e, and Figure S11).

We find the dynamics of the UM at 515 nm (black, Figure 5c) and the dynamics of the DS inside the P3HT cavity at the same wavelength (red dotted, Figure 5c) are the same. In contrast, the dynamics of the DS inside the P3HT/C_{60} bilayer cavity (Figure 5f, red dotted) feature an additional decay after 25 ps, when compared to the UM dynamics. Because this additional decay does not appear in similar analysis of the P3HT cavity (Figure 5c), its origin is related to the presence of the acceptor layer.

The spectroscopic differences between the P3HT and P3HT/C_{60} bilayer cavities provide evidence of an additional decay pathway for the LP state in the bilayer cavity. In contrast to the dominant LP fluorescence band in the P3HT cavity, the bilayer cavity fluorescence is dominated by the contribution from uncoupled molecules (Figure 2d,e). All cavity samples were fabricated under the same conditions. The notable

https://doi.org/10.1021/acs.jpclett.1c02644
J. Phys. Chem. Lett. 2021, 12, 9774−9782

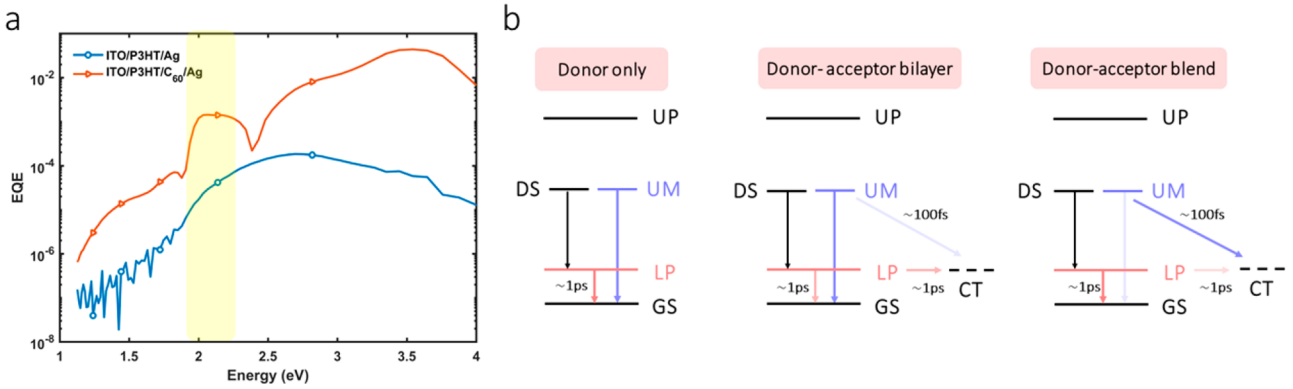

Figure 6. (a) External quantum efficiency spectrum of P3HT/C_{60} bilayer cavity device (brown line) and P3HT only cavity device (blue line). The LP energy region is highlighted in yellow. The P3HT only cavity device has a peak at 2.7 eV but fails to show a featured contribution in the LP energy region as is present in the bilayer cavity device. The bilayer cavity device EQE spectrum has a band around 2.5−3.0 eV corresponding to the P3HT UP states. The second EQE band around 1.9−2.4 eV nm most likely has contributions from C_{60} molecular absorption and P3HT LP states. The feature at higher energies has contributions mostly from P3HT LP and P3HT/C_{60} CT states.[51] In the presence of an acceptor, the LP states participate in photocurrent generation, which is consistent with the observation from transient absorption measurements. (b) Schematic summarizing the relevant decay pathways of the LP and UM in each of the cavity systems. Darker lines indicate more dominant transitions.

difference in fluorescence spectra suggests that the acceptor layer, when present in the resonant cavity, provides a significant additional decay pathway for the LP state. We also note the inversion of the dominant fluorescent species from the LP to the UM as the resonance condition is achieved, suggesting the cavity resonance is a key factor causing the decrease in LP fluorescence (Figure S4).

In an ideal system, all LP fluorescence would be quenched by charge transfer to the acceptor. In a recent study, for example, where both the donor and acceptor were coupled to a cavity mode, the authors concluded that the complete disappearance of the LP fluorescence in the donor−acceptor cavity was a result of the deactivation route provided by the donor−acceptor interface.[47] In such an ideal case, charge transfer from the LP to the acceptor would be significantly faster than the decay of the LP to the ground state. However, as a result of the reduced wave function overlap between the delocalized polariton and the acceptor, we anticipate slower charge transfer from the LP.[36] Specifically, when excitation of an electron donor is strongly delocalized over N molecules, and the electron acceptor lies close to one of the N donor molecular subunits, then the electron transfer matrix element is limited by the wave function amplitude at a single donor site. Therefore, for ideal delocalization, the matrix element is reduced by the factor $1/\sqrt{N}$.

Charge transfer between P3HT and PCBM in annealed blends outside of the cavity occurs on the time scale of hundreds of femtoseconds.[48,49] Inside a cavity, charge transfer from the LP state is slowed to a rate comparable with the lifetime of the LP state (~1 ps, Figure 5a,d). In the bilayer cavity, we observe a small contribution from the LP to the fluorescence, suggesting the decay of the LP to the ground state and the decay of the LP through charge transfer to the acceptor are competing pathways occurring on similar time scales. The slower time scale for LP charge transfer is also supported in the case of the blend cavity fluorescence where the UM fluorescence is quenched more efficiently than the LP fluorescence (Figure 2f). Both the bilayer and blend cavities have two competing pathways for charge transfer to the acceptor: charge transfer from the highly delocalized LP state and charge transfer from the more localized P3HT state (UM). Because the alternative decay pathway to charge transfer is fluorescence for both the LP and the UM, the dominant contributor to the fluorescence spectra for the cavity systems is the less dominant contributor to charge transfer. The bilayer is designed to be nonoptimal for charge transfer from the P3HT state (UM) with a P3HT layer thickness that is significantly greater than the exciton diffusion length of P3HT. In contrast, the blend is optimal for charge transfer from the P3HT state (UM) with a bulk heterojunction architecture where the P3HT and PCBM domains are intermixed providing a donor−acceptor interface within the exciton diffusion length for P3HT for all excitons. Because charge transfer from the more localized P3HT state (UM) is faster than charge transfer from the delocalized LP, we observe more efficient quenching of the UM fluorescence in the blend cavity. As a result of the more efficient quenching of the UM fluorescence, we observe an LP-dominant fluorescence spectrum (Figure 2f) in the blend cavity.

We find further evidence for the additional decay pathway of the LP in the transient dynamics of the DS in the bilayer cavity. The DS of the bilayer cavity show an additional decay after ~25 ps that is not present in the UM dynamics (Figure 5f). A decay from the DS to the LP within 25 ps is a reasonable time scale (Supporting Information), suggesting that after 25 ps we are observing the additional decay pathway of the LP through these DS dynamics.[50] The transient dynamics for P3HT reflect the dynamics of the nonfluorescent states; therefore, the additional decay pathway we observe is also a nonfluorescent decay pathway,[48] which is consistent with charge transfer to the acceptor. Furthermore, the additional decay is not present in the DS dynamics of the P3HT cavity (Figure 5c), indicating it is related to the presence of the acceptor.

The conclusions from transient reflection spectroscopy are also supported with the observation of LP participation in photocurrent generation in external quantum efficiency (EQE) measurements of a bilayer cavity device (Figure 6a). The donor-only and donor−acceptor bilayer cavity systems were made into devices by using patterned reflective electrodes in replacement of the 30 nm solid silver layers. In the bilayer cavity device (Figure 6a, brown line), we find an EQE band with contributions from the LP that is not present in the donor-only cavity device (Figure 6a, blue line). It is the presence of the acceptor that leads to both the appearance of

https://doi.org/10.1021/acs.jpclett.1c02644
J. Phys. Chem. Lett. 2021, 12, 9774−9782

the additional decay pathway for the LP in transient absorption measurements and the participation of the LP in photocurrent generation in EQE measurements. The generation of photocurrent through charge transfer to the acceptor is thus the additional decay pathway for the LP in the bilayer cavity. While the device is not optimized for solar cell efficiency and the resonance condition is altered by the weakly reflective bottom electrode (Figure S14), the EQE measurements serve to confirm that the additional decay pathway for the LP is charge transfer.

In Figure 6b, we summarize the decay pathways for the UM and LP states in each of the cavity systems. In the donor-only system, the LP and the UM decay to the ground state (GS). In both the bilayer and blend cavity systems, there is an additional pathway through charge transfer (CT) for the UM and the LP. The UM excitons that reach the donor−acceptor interface undergo charge transfer in ∼100 fs, which is significantly faster than the ∼1 ps time scale for charge transfer from the LP. In the blend cavity system where all UM excitons reach the donor−acceptor interface, the CT pathway is dominated by UM due to the faster time constant for CT from UM. In contrast, in the bilayer cavity system, the rate of CT from the LP competes with the rate of the decay of the LP to the GS rather than the rate of CT from UM because most excitons formed from UM will not reach the interface. The benefit of the delocalization of the LP is that it can aid in transporting a greater number of excitons to the donor−acceptor interface. As we have demonstrated, this delocalization also slows the rate of CT from a polariton. The LP thus offers no benefit in the blend where the donor and acceptor are intermixed such that all excitons are formed within the exciton diffusion length of a donor−acceptor interface. It is only in the bilayer that we can clearly observe the pathway for the LP to CT because most excitons formed from UM do not reach the interface.

Through a spectroscopic comparison of P3HT, P3HT/C_{60} bilayer, and P3HT:PCBM blend cavity systems, we have shown the presence of the acceptor layer in the bilayer cavity configuration opens an additional decay pathway for the LP through charge transfer. As anticipated, the rate of charge transfer from the polariton is slowed relative to the rate of charge transfer from an uncoupled P3HT molecule, but we have demonstrated that charge transfer remains fast enough to compete with the decay of the LP to the ground state. For the combination of P3HT and a fullerene acceptor, charge transfer from the LP is not optimized to compete with the rate of charge transfer between blended donor and acceptor molecules. However, the properties of the LP, including the lifetime, the photonic and molecular composition, the delocalization, and the energy level, can be tuned by using different materials, resonance conditions, and molecular concentrations;[7,10,52−54] thus, it is possible to enhance exciton transport and charge transfer from an LP state by using more ordered donor materials and different donor−acceptor molecule combinations.

■ ASSOCIATED CONTENT

Supporting Information

The Supporting Information is available free of charge at https://pubs.acs.org/doi/10.1021/acs.jpclett.1c02644.

Experimental details, angle-dependent reflectivity and coupled oscillator model, fluorescence excitation spectra, bare film transient absorption data, off-resonant cavity fluorescence and transient reflectivity, half-cavity dynamics, blend cavity dark state dynamics, cavity device absorption, dark state to lower polariton rate calculation (PDF)

■ AUTHOR INFORMATION

Corresponding Author

Gregory D. Scholes − *Department of Chemistry, Princeton University, Princeton, New Jersey 08544, United States;* orcid.org/0000-0003-3336-7960; Email: gscholes@princeton.edu

Authors

Courtney A. DelPo − *Department of Chemistry, Princeton University, Princeton, New Jersey 08544, United States;* orcid.org/0000-0002-2885-269X

Saeed-Uz-Zaman Khan − *Department of Electrical and Computer Engineering, Princeton University, Princeton, New Jersey 08544, United States*

Kyu Hyung Park − *Department of Chemistry, Princeton University, Princeton, New Jersey 08544, United States*

Bryan Kudisch − *Department of Chemistry, Princeton University, Princeton, New Jersey 08544, United States;* orcid.org/0000-0003-3352-5383

Barry P. Rand − *Department of Electrical and Computer Engineering and Andlinger Center for Energy and the Environment, Princeton University, Princeton, New Jersey 08544, United States;* orcid.org/0000-0003-4409-8751

Complete contact information is available at: https://pubs.acs.org/10.1021/acs.jpclett.1c02644

Author Contributions

S.-U.-Z.K. and K.H.P. contributed equally to this work.

Notes

The authors declare no competing financial interest.

■ ACKNOWLEDGMENTS

This research was funded by the Gordon and Betty Moore Foundation through Grant GBMF7114. S.U.Z.K. and B.P.R. acknowledge funding from the U.S. Department of Energy, Office of Basic Energy Sciences, Division of Materials Sciences and Engineering, under Award DE-SC0012458. B.K. acknowledges support by the National Science Foundation Graduate Research Fellowship under Grant DGE-1656466. The authors acknowledge the use of Princeton's Imaging and Analysis Center, which is partially supported through the Princeton Center for Complex Materials (PCCM), a National Science Foundation (NSF)-MRSEC program (DMR-2011750). This research made use of the PRISM Cleanroom at Princeton University. We acknowledge Anoop Thomas, Kalaivanan Nagarajan, and Thibault Chervy for sharing their P3HT cavity fabrication conditions and Thomas Ebbesen for providing valuable comments on the work.

■ REFERENCES

(1) Coles, D. M.; Somaschi, N.; Michetti, P.; Clark, C.; Lagoudakis, P. G.; Savvidis, P. G.; Lidzey, D. G. Polariton-Mediated Energy Transfer between Organic Dyes in a Strongly Coupled Optical Microcavity. *Nat. Mater.* **2014**, *13* (7), 712−719.

(2) Zhong, X.; Chervy, T.; Zhang, L.; Thomas, A.; George, J.; Genet, C.; Hutchison, J. A.; Ebbesen, T. W. Energy Transfer between Spatially Separated Entangled Molecules. *Angew. Chem., Int. Ed.* **2017**, *56* (31), 9034−9038.

(3) Zhong, X.; Chervy, T.; Wang, S.; George, J.; Thomas, A.; Hutchison, J. A.; Devaux, E.; Genet, C.; Ebbesen, T. W. Non-Radiative Energy Transfer Mediated by Hybrid Light-Matter States. *Angew. Chem., Int. Ed.* **2016**, *55* (21), 6202−6206.
(4) Tian, M.; Li, X.; Li, Z.; Zhong, X. Analysis of the Forward and Reverse Strongly Coupled States on the Nonradiative Energy Transfer Effect. *J. Phys. Chem. Lett.* **2021**, *12* (20), 4944−4950.
(5) Nagarajan, K.; George, J.; Thomas, A.; Devaux, E.; Chervy, T.; Azzini, S.; Joseph, K.; Jouaiti, A.; Hosseini, M. W.; Kumar, A.; Genet, C.; Bartolo, N.; Ciuti, C.; Ebbesen, T. W. Conductivity and Photoconductivity of a P-Type Organic Semiconductor under Ultrastrong Coupling. *ACS Nano* **2020**, *14* (8), 10219−10225.
(6) Orgiu, E.; George, J.; Hutchison, J. A.; Devaux, E.; Dayen, J. F.; Doudin, B.; Stellacci, F.; Genet, C.; Schachenmayer, J.; Genes, C.; Pupillo, G.; Samorì, P.; Ebbesen, T. W. Conductivity in Organic Semiconductors Hybridized with the Vacuum Field. *Nat. Mater.* **2015**, *14* (11), 1123−1129.
(7) Yu, Y.; Mallick, S.; Wang, M.; Börjesson, K. Barrier-Free Reverse-Intersystem Crossing in Organic Molecules by Strong Light-Matter Coupling. *Nat. Commun.* **2021**, *12* (1), 3255.
(8) Stranius, K.; Hertzog, M.; Börjesson, K. Selective Manipulation of Electronically Excited States through Strong Light−Matter Interactions. *Nat. Commun.* **2018**, *9* (1), 2273.
(9) Scholes, G. D. Polaritons and Excitons: Hamiltonian Design for Enhanced Coherence. *Proc. R. Soc. London, Ser. A* **2020**, *476* (2242), 20200278.
(10) Ebbesen, T. W. Hybrid Light−Matter States in a Molecular and Material Science Perspective. *Acc. Chem. Res.* **2016**, *49* (11), 2403−2412.
(11) Scholes, G. D.; DelPo, C. A.; Kudisch, B. Entropy Reorders Polariton States. *J. Phys. Chem. Lett.* **2020**, *11*, 6389.
(12) Rozenman, G. G.; Akulov, K.; Golombek, A.; Schwartz, T. Long-Range Transport of Organic Exciton-Polaritons Revealed by Ultrafast Microscopy. *ACS Photonics* **2018**, *5* (1), 105−110.
(13) Hagenmüller, D.; Schachenmayer, J.; Schütz, S.; Genes, C.; Pupillo, G. Cavity-Enhanced Transport of Charge. *Phys. Rev. Lett.* **2017**, *119* (22), 223601.
(14) Schachenmayer, J.; Genes, C.; Tignone, E.; Pupillo, G. Cavity-Enhanced Transport of Excitons. *Phys. Rev. Lett.* **2015**, *114* (19), 196403.
(15) Feist, J.; Garcia-Vidal, F. J. Extraordinary Exciton Conductance Induced by Strong Coupling. *Phys. Rev. Lett.* **2015**, *114* (19), 196402.
(16) Yao, N.; Wang, J.; Chen, Z.; Bian, Q.; Xia, Y.; Zhang, R.; Zhang, J.; Qin, L.; Zhu, H.; Zhang, Y.; Zhang, F. Efficient Charge Transport Enables High Efficiency in Dilute Donor Organic Solar Cells. *J. Phys. Chem. Lett.* **2021**, *12* (20), 5039−5044.
(17) Oh, C.-M.; Lee, J.; Park, S. H.; Hwang, I.-W. Enhanced Charge Separation in Ternary Bulk-Heterojunction Organic Solar Cells by Fullerenes. *J. Phys. Chem. Lett.* **2021**, *12* (27), 6418−6424.
(18) Verreet, B.; Heremans, P.; Stesmans, A.; Rand, B. P. Microcrystalline Organic Thin-Film Solar Cells. *Adv. Mater.* **2013**, *25* (38), 5504−5507.
(19) Morfa, A. J.; Rowlen, K. L.; Reilly, T. H.; Romero, M. J.; van de Lagemaat, J. Plasmon-Enhanced Solar Energy Conversion in Organic Bulk Heterojunction Photovoltaics. *Appl. Phys. Lett.* **2008**, *92* (1), 013504.
(20) Garnett, E. C.; Ehrler, B.; Polman, A.; Alarcon-Llado, E. Photonics for Photovoltaics: Advances and Opportunities. *ACS Photonics* **2021**, *8* (1), 61−70.
(21) Lee, J.-Y.; Connor, S. T.; Cui, Y.; Peumans, P. Solution-Processed Metal Nanowire Mesh Transparent Electrodes. *Nano Lett.* **2008**, *8* (2), 689−692.
(22) Polman, A.; Atwater, H. A. Photonic Design Principles for Ultrahigh-Efficiency Photovoltaics. *Nat. Mater.* **2012**, *11* (3), 174−177.
(23) Paz-Soldan, D.; Lee, A.; Thon, S. M.; Adachi, M. M.; Dong, H.; Maraghechi, P.; Yuan, M.; Labelle, A. J.; Hoogland, S.; Liu, K.; Kumacheva, E.; Sargent, E. H. Jointly Tuned Plasmonic−Excitonic Photovoltaics Using Nanoshells. *Nano Lett.* **2013**, *13* (4), 1502−1508.
(24) Wang, J.; Lee, Y.-J.; Chadha, A. S.; Yi, J.; Jespersen, M. L.; Kelley, J. J.; Nguyen, H. M.; Nimmo, M.; Malko, A. V.; Vaia, R. A.; Zhou, W.; Hsu, J. W. P. Effect of Plasmonic Au Nanoparticles on Inverted Organic Solar Cell Performance. *J. Phys. Chem. C* **2013**, *117* (1), 85−91.
(25) Bonin, G. O.; Barrow, S. J.; Connell, T. U.; Roberts, A.; Chesman, A. S. R.; Gómez, D. E. Self-Assembly of Plasmonic Near-Perfect Absorbers of Light: The Effect of Particle Size. *J. Phys. Chem. Lett.* **2020**, *11* (19), 8378−8385.
(26) Rand, B. P.; Genoe, J.; Heremans, P.; Poortmans, J. Solar Cells Utilizing Small Molecular Weight Organic Semiconductors. *Prog. Photovoltaics* **2007**, *15* (8), 659−676.
(27) Mikhnenko, O. V.; Blom, P. W. M.; Nguyen, T.-Q. Exciton Diffusion in Organic Semiconductors. *Energy Environ. Sci.* **2015**, *8* (7), 1867−1888.
(28) Tang, C. W. Two-layer Organic Photovoltaic Cell. *Appl. Phys. Lett.* **1986**, *48* (2), 183−185.
(29) Menke, S. M.; Holmes, R. J. Exciton Diffusion in Organic Photovoltaic Cells. *Energy Environ. Sci.* **2014**, *7* (2), 499−512.
(30) Chen, D.; Nakahara, A.; Wei, D.; Nordlund, D.; Russell, T. P. P3HT/PCBM Bulk Heterojunction Organic Photovoltaics: Correlating Efficiency and Morphology. *Nano Lett.* **2011**, *11* (2), 561−567.
(31) van Bavel, S. S.; Bärenklau, M.; de With, G.; Hoppe, H.; Loos, J. P3HT/PCBM Bulk Heterojunction Solar Cells: Impact of Blend Composition and 3D Morphology on Device Performance. *Adv. Funct. Mater.* **2010**, *20* (9), 1458−1463.
(32) Deibel, C.; Dyakonov, V.; Brabec, C. J. Organic Bulk-Heterojunction Solar Cells. *IEEE J. Sel. Top. Quantum Electron.* **2010**, *16* (6), 1517−1527.
(33) Tamai, Y.; Ohkita, H.; Benten, H.; Ito, S. Exciton Diffusion in Conjugated Polymers: From Fundamental Understanding to Improvement in Photovoltaic Conversion Efficiency. *J. Phys. Chem. Lett.* **2015**, *6* (17), 3417−3428.
(34) Eizner, E.; Martínez-Martínez, L. A.; Yuen-Zhou, J.; Kéna-Cohen, S. Inverting Singlet and Triplet Excited States Using Strong Light-Matter Coupling. *Sci. Adv.* **2019**, *5* (12), No. eaax4482.
(35) Martínez-Martínez, L. A.; Eizner, E.; Kéna-Cohen, S.; Yuen-Zhou, J. Triplet Harvesting in the Polaritonic Regime: A Variational Polaron Approach. *J. Chem. Phys.* **2019**, *151* (5), 054106.
(36) Ye, C.; Mallick, S.; Hertzog, M.; Kowalewski, M.; Börjesson, K. Direct Transition from Triplet Excitons to Hybrid Light−Matter States via Triplet−Triplet Annihilation. *J. Am. Chem. Soc.* **2021**, *143* (19), 7501−7508.
(37) Clark, J.; Silva, C.; Friend, R. H.; Spano, F. C. Role of Intermolecular Coupling in the Photophysics of Disordered Organic Semiconductors: Aggregate Emission in Regioregular Polythiophene. *Phys. Rev. Lett.* **2007**, *98* (20), 206406.
(38) Spano, F. C. Modeling Disorder in Polymer Aggregates: The Optical Spectroscopy of Regioregular Poly(3-Hexylthiophene) Thin Films. *J. Chem. Phys.* **2005**, *122* (23), 234701.
(39) Kramer, S. N.; Brown, J.; Rice, M.; Peteanu, L. A. Unraveling the Contribution of Residual Monomer to the Emission Spectra of Poly(3-Hexylthiophene) Aggregates: Implications for Identifying H- and J-Type Coupling. *J. Phys. Chem. Lett.* **2021**, *12*, 5919−5924.
(40) Cook, S.; Ohkita, H.; Kim, Y.; Benson-Smith, J. J.; Bradley, D. D. C.; Durrant, J. R. A Photophysical Study of PCBM Thin films. *Chem. Phys. Lett.* **2007**, *445*, 276.
(41) Krätschmer, W.; Lamb, L. D.; Fostiropoulos, K.; Huffman, D. R. Solid C60: A New Form of Carbon. *Nature* **1990**, *347* (6291), 354−358.
(42) Shaw, P. E.; Ruseckas, A.; Samuel, I. D. W. Exciton Diffusion Measurements in Poly(3-Hexylthiophene). *Adv. Mater.* **2008**, *20* (18), 3516−3520.
(43) Garcia-Vidal, F. J.; Ciuti, C.; Ebbesen, T. W. Manipulating Matter by Strong Coupling to Vacuum Fields. *Science* **2021**, *373* (6551), No. eabd0336.
(44) Qiu, L.; Mandal, A.; Morshed, O.; Meidenbauer, M. T.; Girten, W.; Huo, P.; Vamivakas, A. N.; Krauss, T. D. Molecular Polaritons Generated from Strong Coupling between CdSe Nanoplatelets and a

https://doi.org/10.1021/acs.jpclett.1c02644
J. Phys. Chem. Lett. 2021, 12, 9774−9782

Dielectric Optical Cavity. *J. Phys. Chem. Lett.* **2021**, *12* (20), 5030−5038.
(45) Schwartz, T.; Hutchison, J. A.; Léonard, J.; Genet, C.; Haacke, S.; Ebbesen, T. W. Polariton Dynamics under Strong Light-Molecule Coupling. *ChemPhysChem* **2013**, *14* (1), 125−131.
(46) DelPo, C. A.; Kudisch, B.; Park, K. H.; Khan, S.-U.-Z.; Fassioli, F.; Fausti, D.; Rand, B. P.; Scholes, G. D. Polariton Transitions in Femtosecond Transient Absorption Studies of Ultrastrong Light−Molecule Coupling. *J. Phys. Chem. Lett.* **2020**, *11*, 2667−2674.
(47) Wang, M.; Hertzog, M.; Börjesson, K. Polariton-Assisted Excitation Energy Channeling in Organic Heterojunctions. *Nat. Commun.* **2021**, *12* (1), 1874.
(48) Piris, J.; Dykstra, T. E.; Bakulin, A. A.; van Loosdrecht, P. H. M.; Knulst, W.; Trinh, M. T.; Schins, J. M.; Siebbeles, L. D. A. Photogeneration and Ultrafast Dynamics of Excitons and Charges in P3HT/PCBM Blends. *J. Phys. Chem. C* **2009**, *113* (32), 14500−14506.
(49) Marsh, R. A.; Hodgkiss, J. M.; Albert-Seifried, S.; Friend, R. H. Effect of Annealing on P3HT:PCBM Charge Transfer and Nanoscale Morphology Probed by Ultrafast Spectroscopy. *Nano Lett.* **2010**, *10* (3), 923−930.
(50) Agranovich, V. M.; Litinskaia, M.; Lidzey, D. G. Cavity Polaritons in Microcavities Containing Disordered Organic Semiconductors. *Phys. Rev. B: Condens. Matter Mater. Phys.* **2003**, *67* (8), 085311.
(51) Vandewal, K.; Tvingstedt, K.; Gadisa, A.; Inganäs, O.; Manca, J. V. Relating the Open-Circuit Voltage to Interface Molecular Properties of Donor:Acceptor Bulk Heterojunction Solar Cells. *Phys. Rev. B: Condens. Matter Mater. Phys.* **2010**, *81* (12), 125204.
(52) Liu, B.; Menon, V. M.; Sfeir, M. Y. The Role of Long-Lived Excitons in the Dynamics of Strongly Coupled Molecular Polaritons. *ACS Photonics* **2020**, *7* (8), 2292−2301.
(53) Hertzog, M.; Wang, M.; Mony, J.; Börjesson, K. Strong Light−Matter Interactions: A New Direction within Chemistry. *Chem. Soc. Rev.* **2019**, *48* (3), 937−961.
(54) Gu, B.; Mukamel, S. Optical-Cavity Manipulation of Conical Intersections and Singlet Fission in Pentacene Dimers. *J. Phys. Chem. Lett.* **2021**, *12* (8), 2052−2056.

https://doi.org/10.1021/acs.jpclett.1c02644
J. Phys. Chem. Lett. 2021, 12, 9774−9782